Spin-state transition in $Ba_2Co_9O_{14}$

J.-G. Cheng,[1] J.-S. Zhou,[1,*] Z. Hu,[2,†] M. R. Suchomel,[3] Y. Y. Chin,[2] C. Y. Kuo,[2] H.-J. Lin,[4] J. M. Chen,[4] D. W. Pi,[4] C. T. Chen,[4] T. Takami,[5] L. H. Tjeng,[2] and J. B. Goodenough[1]

[1]*Materials Science and Engineering Program/Mechanical Engineering, University of Texas at Austin, Austin, Texas 78712, USA*

[2]*Max Planck Institute for Chemical Physics of Solids, Nöthnitzerstr, 40, D-01187 Dresden, Germany*

[3]*Advanced Photon Source, Argonne National Laboratory, Argonne, Illinois 60439, USA*

[4]*National Synchrotron Radiation Research Center, HsinChu 30077, Taiwan*

[5]*Department of Physics, Graduate School of Science, Osaka University, 1-1 Machikaneyama-cho, Toyonaka, Osaka 560-0043, Japan*

(Received 18 January 2012; revised manuscript received 12 March 2012; published 23 March 2012)

$Ba_2Co_9O_{14}$ is a charge-ordered $Co^{2+/3+}$ cobaltite that consists of building blocks of CdI_2-type $Co^{2+/3+}O_{6/3}$ layers, face-shared $Co^{3+}{}_3O_{12}$ octahedral trimers, and corner-sharing $Co^{2+}O_4$ tetrahedra. The Co-$L_{2,3}$ x-ray absorption spectroscopy spectrum at room temperature indicates a high and a low spin state for Co^{2+} and Co^{3+} ions, respectively. Measurements of high-temperature resistivity and thermoelectric power revealed an insulator-to-insulator phase transition at $T_t = 570$ K, above which the inverse magnetic susceptibility $\chi^{-1}(T)$ deviates from the Curie-Weiss law. By using a combination of soft x-ray absorption spectroscopy at the O-K edge and high-resolution synchrotron x-ray powder diffraction measurements on crossing T_t, we have successfully determined the origin of this phase transition as a low-to-higher spin-state transition of Co^{3+} ions within the face-shared Co_3O_{12} octahedral trimers in $Ba_2Co_9O_{14}$.

DOI: 10.1103/PhysRevB.85.094424 PACS number(s): 75.25.−j, 71.30.+h, 71.27.+a, 78.70.Dm

I. INTRODUCTION

Layered cobalt oxides have attracted renewed interest in recent years because of the observations of promising thermoelectric properties in Na_xCoO_2[1] and superconductivity in the bilayer hydrated $Na_{0.35}CoO_2{\cdot}1.3H_2O$.[2] The crystal structure of Na_xCoO_2 can be described as alternate stacking of CdI_2-type $CoO_{6/3}$ layers with randomly distributed Na layers. Extensive investigations have led to the identification of several misfit-layered cobaltites such as $[Ca_2CoO_3][CoO_2]_{1.62}$[3] and $[Pb_{0.7}Sr_{1.9}Co_{0.4}O_3][CoO_2]_{1.8}$;[4] they all have a similar mixed-valent CdI_2-type $Co^{3+/4+}O_{6/3}$ layer and exhibit a relatively high thermoelectric power and a low resistivity. In addition to charge and orbital degrees of freedom, the cobaltites containing Co^{3+} at octahedral sites exhibit different spin states, i.e., a low spin (LS, $t_{2g}^6e_g^0$, $S = 0$), a high spin (HS, $t_{2g}^4e_g^2$, $S = 2$), and even an intermediate spin (IS, $t_{2g}^5e_g^1$, $S = 1$) state.[5,6] Spin-state transitions are generally believed to be associated with the unconventional transport properties of cobaltites[7] and the spin-blockade phenomena found in $RBaCo_2O_{5.5}$[8–11] and the $La_{2-x}Sr_xCoO_4$ series.[12]

Recently, Sun *et al.*[13] reported the synthesis and crystal structure of a barium cobaltite $Ba_2Co_9O_{14}$ that also contains CdI_2-type $CoO_{6/3}$ layers. However, it is an insulator below room temperature and orders antiferromagnetically below $T_N \approx 40$ K. The detailed magnetic structure of $Ba_2Co_9O_{14}$ was subsequently investigated by Ehora *et al.*[14] using neutron diffraction. Figure 1 displays the crystal structure of $Ba_2Co_9O_{14}$, which can be described as an intergrowth of CdI_2-type $CoO_{6/3}$ layers and Co_3O_{12} octahedral trimers that are interconnected by corner-sharing CoO_4 tetrahedra. As shown in Fig. 1, there are five crystallographically independent Co sites in two types of coordination polyhedra: the Co2 octahedron shares its opposite triangular faces with two Co1 octahedra, forming the Co_3O_{12} octahedral trimer; the Co4 and Co5 octahedra share edges to form the CdI_2-type layer, with a 2:1 ordered arrangement within a two-dimensional triangular lattice; and the Co3 tetrahedron shares corners with both the Co_3O_{12} trimers and the CdI_2 layers. Co1, Co2, and Co4 ions are trivalent (Co^{3+}) and diamagnetic in a LS state, while Co3 and Co5 ions are divalent (Co^{2+}) with a HS configuration ($S = 3/2$). These HS Co^{2+} ions in the matrix of LS Co^{3+} ions are coupled through Co-O-O-Co "superexchange" interactions, which give rise to a complex antiferromagentic ordering below $T_N \approx 40$ K.[14] Given that the LS Co^{3+} ions within the Co_3O_{12} octahedral trimers do not contribute to the electronic conduction, a charge ordering of the trivalent Co4 and divalent Co5 sites within the CdI_2 layers makes $Ba_2Co_9O_{14}$ an insulator, which is in contrast to the conductive mixed-valent $Co^{3+/4+}O_{6/3}$ layers in other layered cobaltites mentioned previously.

Ehora *et al.*[14] have extended the resistivity measurement up to 900 K and observed a broad transition to another insulator phase with a smaller energy gap at $T > T_t \approx 600$ K. They have attributed this change to the creation of oxygen vacancies because their thermogravimetric data exhibited a small weight loss of 0.2 oxygen atoms per formula in the temperature range from room temperature to ∼730 K. However, the phase with a wider energy gap was not recovered when the sample was reoxidized upon further heating above 730 K. This observation indicates that the anomaly of $\rho(T)$ at T_t may have little to do with the change of oxygen concentration. Alternatively, the insulator–insulator transition in $Ba_2Co_9O_{14}$ could be caused by (1) a thermally driven spin-state transition from LS Co^{3+} to higher-spin states at elevated temperatures, like the well-known case of the perovskite $LaCoO_3$,[15] or (2) melting of the charge ordering on the Co4 and Co5 sites within the CdI_2-type layers.

To elucidate the origin of this transition, we comprehensively characterized $Ba_2Co_9O_{14}$ above room temperature through measurements of resistivity, thermoelectric power, magnetic susceptibility, soft x-ray absorption spectroscopy

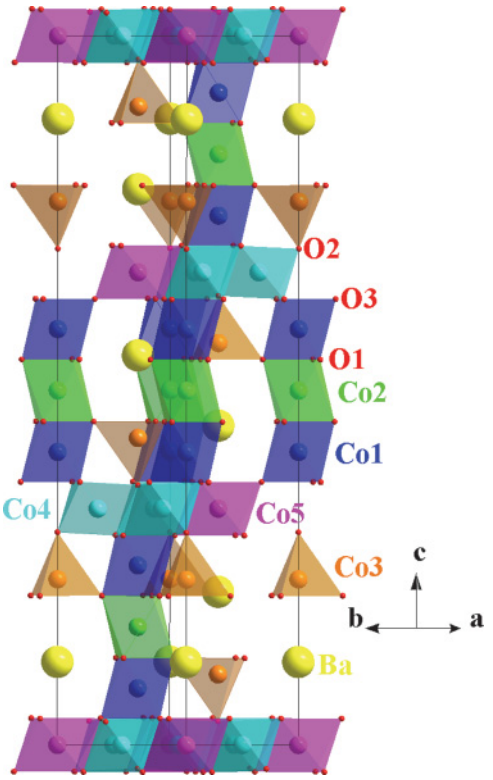

FIG. 1. (Color online) Crystal structure of $Ba_2Co_9O_{14}$. Polyhedra shading (coloring) distinguishes the five crystallographically independent Co sites in the structure.

(XAS) at the Co-$L_{2,3}$ and O-K edges, and high-resolution synchrotron x-ray powder diffraction (SXRD). Our high-temperature resistivity data are nearly identical to those obtained by Ehora *et al.*,[14] which confirms an insulator–insulator transition in our $Ba_2Co_9O_{14}$ sample. However, instead of their proposed electron doping model induced by oxygen deficiency created near T_t, our high-temperature spectroscopy and structural studies support a scenario in which the insulator–insulator transition is due to a low-to-higher spin-state transition of the Co^{3+} ions within the face-shared octahedral trimers.

II. EXPERIMENTAL DETAILS

Polycrystalline $Ba_2Co_9O_{14}$ samples were prepared through a conventional solid-state reaction from a stoichiometric mixture of $BaCO_3$ and Co_3O_4 in air. Details about sample synthesis and characterizations of the physical properties below room temperature can be found elsewhere.[16] The high-temperature resistivity and thermoelectric power were measured simultaneously with a homemade device in the temperature range $300 < T < 773$ K in an Ar atmosphere. Magnetic-susceptibility measurements were carried out in a vacuum of 10^{-3} torr with a commercial superconducting quantum interference device magnetometer (Quantum Design) from 300 to 750 K. These measurements have been performed during heating and cooling. The soft XAS at the Co-$L_{2,3}$ and O-K edges on the polycrystalline $Ba_2Co_9O_{14}$ samples were measured at the BL11A and BL08B beamlines of the National Synchrotron Radiation Research Center in Taiwan. The Co-$L_{2,3}$ and O-K XAS spectra were taken in the total-electron-yield mode and the fluorescence-yield (FY) mode with a photon energy resolution of 0.3 and 0.2 eV, respectively. Clean sample surfaces were obtained by cutting pellets *in situ* just before collecting the data in an ultra-high-vacuum chamber with a pressure in the low 10^{-9}-mbar range. High-resolution SXRD data were collected upon heating from 298 to 872 K on beamline 11-BM ($\lambda = 0.41219$ Å) at the Advanced Photon Source, Argonne National Laboratory.[17] The obtained SXRD patterns were analyzed by the Rietveld method with the FULLPROF program.[18]

III. RESULTS AND DISCUSSION

Figure 2 displays the temperature dependences of resistivity $\rho(T)$ and thermoelectric power $S(T)$ of the $Ba_2Co_9O_{14}$ sample measured on cycling between 300 and 773 K in an Ar atmosphere. In accordance with the report by Ehora *et al.*,[14] our $\rho(T)$ data confirm a broad insulator–insulator transition at T_t. We defined $T_t = 570$ K as the peak temperature in the plot of $d(\ln\rho)/d(1/T)$ vs $1/T$ (inset of Fig. 2). The $\rho(T)$ data measured during heating and cooling overlap one another. The $S(T)$ curve also shows an anomaly near T_t. $S(T)$ is nearly temperature independent at $T < 530$ K, which is typical for a polaronic conductor. Given the insulator–insulator transition deduced from the $\rho(T)$ measurement, a sharp decrease of S at $T > T_t$ indicates that the transition is associated with releasing mobile charge carriers at $T = T_t$. Although the $S(T)$ data measured during cooling overlap those on heating at high temperatures, the sample shows a lower S at $T < T_t$ after one thermal cycle. It is clear that the oxygen concentration for this p-type conductor is slightly reduced during the high-temperature measurement. However, the abrupt mobile charge carrier release near T_t should be distinguished from the gradual charge carrier increase taking place at high temperatures.

Figure 3 displays the paramagnetic susceptibility $\chi(T)$ and its inverse $\chi^{-1}(T)$ upon thermal cycling between 300 and 750 K under an external magnetic field $H = 2$ T. The

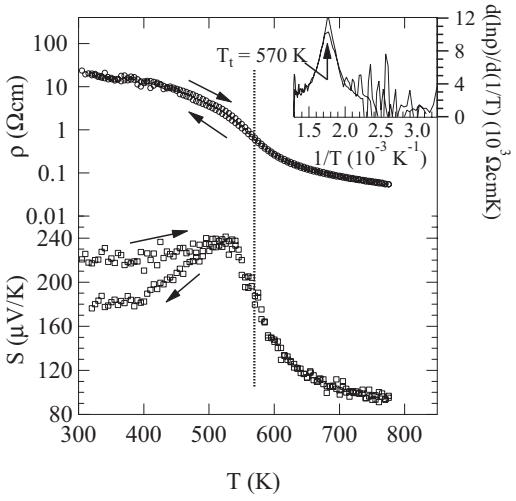

FIG. 2. Temperature dependences of resistivity $\rho(T)$ and thermoelectric power $S(T)$ measured on thermal cycling between 300 and 773 K. Transition temperature $T_t = 570$ K was determined from the peak of $d(\ln\rho)/d(1/T)$ shown in the inset.

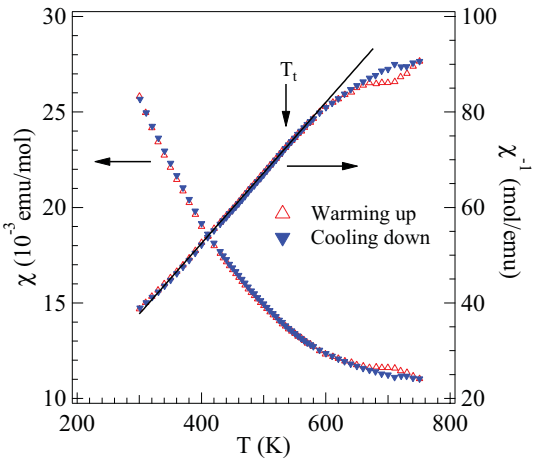

FIG. 3. (Color online) Temperature dependence of the magnetic susceptibility $\chi(T)$ and the inverse $\chi^{-1}(T)$ on heating and cooling between 300 and 750 K. The C-W fitting curve is shown by the solid line.

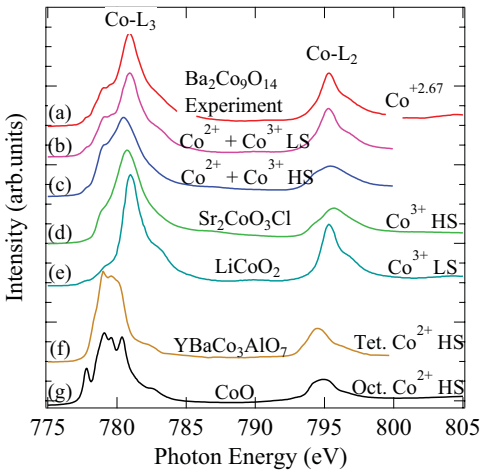

FIG. 4. (Color online) The Co-$L_{2,3}$ XAS spectra of (a) $Ba_2Co_9O_{14}$ and reference compounds, (b) and (c) simulated spectra (see details in the text), (d) Sr_2CoO_3Cl (Ref. 21), (e) $LiCoO_2$ (Ref. 24), (f) $YBaCo_3AlO_7$ (Ref. 25), and (g) CoO, all taken at 300 K.

inverse $\chi^{-1}(T)$ shows nearly linear behavior and no difference for measurements during heating and cooling below 570 K. The slight reduction of oxygen concentration, as seen from the high-temperature $S(T)$ measurement in Fig. 2, does not alter the magnetic properties below T_t. From the Curie-Weiss (C-W) fitting, we obtained an effective paramagnetic moment $\mu_{\text{eff}} = 7.36\ \mu_B$/f.u. and a Weiss temperature $\theta = 44.8$ K within $300 < T < 570$ K. In accordance with the long-range antiferromagentic ordering at $T_N \approx 40$ K, a negative $\theta = -50.9$ K has been obtained by Ehora *et al.*[14] from a C-W fitting to $\chi^{-1}(T)$ below 300 K. But a closer inspection of the $\chi^{-1}(T)$ data in Ehora *et al.*[14] revealed that the slope of $\chi^{-1}(T)$ increases gradually with temperature, which is consistent with a positive θ that we obtained within the temperature range $300 < T < 570$ K. A temperature-dependent Weiss constant may reflect a contribution from unquenched orbital angular momentum, which makes the C-W law invalid in some cases.[19] Ehora *et al.*[14] found that the μ_{eff} from $\chi(T)$ below room temperature is significantly larger than the expected spin-only value of 5.74 μ_B/f.u. for a $S = 3/2$ state on HS Co3 and Co5 sites, which supports an orbital contribution and/or some thermal excitations to a higher spin state. For $T > 570$ K, $\chi^{-1}(T)$ deviates obviously from C-W behavior and a hysteresis loop develops in the temperature range $660 < T < 750$ K. These observations might indicate that some LS Co^{3+} ions at Co1, Co2, and/or Co4 sites are transforming to a higher spin state above 570 K.

To probe directly the valence and spin states of the Co ions in $Ba_2Co_9O_{14}$, we turn to the more sensitive XAS measurements at the Co-$L_{2,3}$ and O-K absorption edges. The Co ($2p \rightarrow 3d$) transitions at the Co-$L_{2,3}$ edge involve directly the relevant valence shell and are extremely sensitive to the charge and spin states. The profile of an XAS spectrum reveals information about the valence and spin states.[9,20–23] First, we checked the valence state and the spin states of Co ions at room temperature by using the Co-$L_{2,3}$ XAS spectrum. Figure 4 displays the room-temperature Co-$L_{2,3}$ XAS spectrum of $Ba_2Co_9O_{14}$, together with that of Sr_2CoO_3Cl,[18] $LiCoO_2$,[24] $YBaCo_3AlO_7$,[25] and CoO that serve as the references for the HS Co^{3+}, the LS Co^{3+}, the tetrahedral-site (Tet.) HS Co^{2+}, and the octahedral-site (Oct.) HS Co^{2+}, respectively. We removed the Ba $M_{4,5}$ white lines located at 784 and 798 eV by using the Ba $M_{4,5}$ spectrum of $YBaZn_3AlO_7$. The Co spectra of the different valence and spin configurations show quite different multiplet structures. We can see that the Co^{2+} spectra of CoO and $YBaCo_3AlO_7$ contain peaks located at least 2 eV below the main peak of the Co^{3+} spectra. While the main peaks for the Co^{2+} spectra lie at ~779 eV, the main peaks for the Co^{3+} spectra lie at 780.5 eV. This difference is consistent with the generally accepted notion that an increase of the valence state from Co^{2+} to Co^{3+}, for example, typically results in a shift of the $L_{2,3}$ XAS spectra to higher energies by 1 eV or more.[9,22] The lowest-energy peak at 777.8 eV is characteristic of octahedral-site Co^{2+}. Compared to the HS Sr_2CoO_3Cl, the LS $LiCoO_2$ has a higher intensity at the L_2 edge, with a rather sharp peak at 795 eV. As for the $Ba_2Co_9O_{14}$ spectrum, the profile can be decomposed into at least two components, one at 777.8 and 779 eV, which is close to Co^{2+} in the reference compound CoO, and another at 795 eV for the Co-L_2 edge from LS Co^{3+}. These observations strongly suggest the presence of Co^{2+} and LS Co^{3+} ions in this material, which is highly consistent with results from previous neutron powder diffraction (NPD) refinements.[14] To further verify this hypothesis, we carried out a simulation by adding spectra from the as-measured CoO, $YBaCo_3AlO_7$, and $LiCoO_2$ with a ratio of 2/9 Co^{2+} (Tet.) + 1/9 Co^{2+} (Oct.) + 6/9 Co^{3+} (Oct.) and compared the result with that of $Ba_2Co_9O_{14}$. As seen in Fig. 4, the match between the experimental spectrum and the simulated one is nearly perfect. In contrast, the simulated spectrum is quite different from that of $Ba_2Co_9O_{14}$ if the spectrum from $LiCoO_2$ is replaced by that of Sr_2CoO_3Cl; the difference becomes more prominent at the L_2 edge. Therefore, the Co-$L_{2,3}$ XAS results establish that all Co^{3+} ions in $Ba_2Co_9O_{14}$ are in the LS state at room temperature.

After clarifying the valence and spin states on the cobalt sites at room temperature, we investigate the possibility

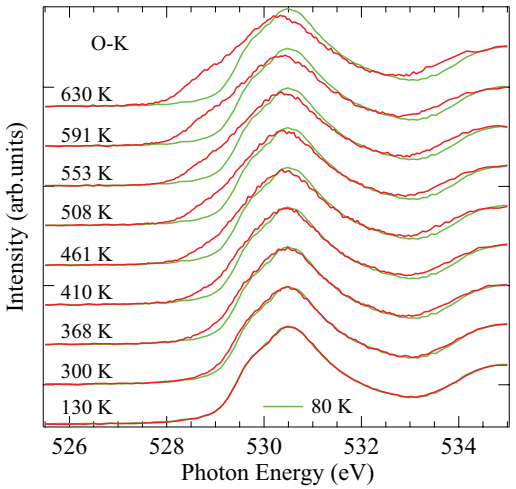

FIG. 5. (Color online) Temperature-dependent O-K XAS spectra of $Ba_2Co_9O_{14}$. The light gray (green) line at each temperature is taken at 80 K for comparison.

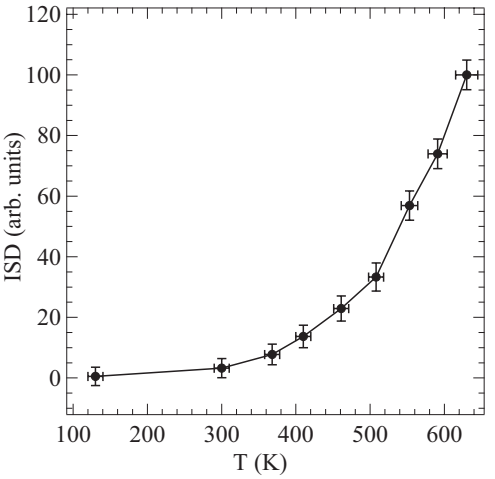

FIG. 6. Temperature dependence of ISD from the pre-edge peak in the O-K XAS spectra of $Ba_2Co_9O_{14}$.

of a spin-state transition as the temperature increases by using the O-K XAS spectrum, which was measured with a bulk-sensitive FY method. The advantage of the FY O-K XAS spectrum is that it allows us to minimize the signal from the sample surface where some oxygen might be lost to the vacuum at high temperatures. Figure 5 displays the temperature-dependent O-K XAS spectra of $Ba_2Co_9O_{14}$. Here, we are mainly interested in the lowest-lying states, i.e., the unoccupied states related to the Co^{3+} ions.[9,18,26] These states are located at the pre-edge region below 532 eV and originated from transitions from the O 1s core level to the O 2p orbitals that are mixed into the unoccupied Co 3d states.[9,18,19,23] For a LS Co^{3+} below 300 K with the $t_{2g}^6e_g^0$ configuration, the lowest-energy structure in the O-K spectrum ~530.5 eV is due to the transitions from the O1s core level into the unoccupied Co 3d e_g states, because the low-lying t_{2g} orbitals are fully occupied. However, as the temperature increases to above room temperature, a lower-energy spectral feature ~528.7 eV appears and becomes very pronounced above 510 K, whereas the peak at 530.5 eV loses its spectral weight. These temperature-dependent spectral changes are due to a spin-state transition of Co^{3+}, similar to that observed in $LaCoO_3$,[23] and reflect that transitions to the lower-lying t_{2g} orbitals are now allowed, i.e., the t_{2g} states are no longer fully occupied. In other words, at $T > 300$ K, some LS Co^{3+} ions in $Ba_2Co_9O_{14}$ transform into the HS $t_{2g}^4e_g^2$ or IS $t_{2g}^5e_g^1$ state.

To have a quantitative description of the temperature-dependent spectral-weight transfer, we present in Fig. 6 the temperature-dependent ISD from the O-K XAS, where ISD is the integration of signal $|I(T) - I(80\ \mathrm{K})|^2$, in which $I(80\ \mathrm{K})$ and $I(T)$ refer to the spectral intensity from 526.6 to 532.6 eV at 80 K and at temperatures above 80 K, respectively. From Fig. 6, we can see a dramatic increase of the ISD signal at $T > 550$ K, reflecting an accelerated spin-state transition of Co^{3+}, in agreement with the observed anomalies in transport and magnetic properties in Figs. 1 and 2. In comparison with $LaCoO_3$, the spectral weight transfer from an e_g- to a t_{2g}-related peak in the interval $80 < T < 630$ K in the $Ba_2Co_9O_{14}$ spectra is weaker, indicating that there are fewer Co^{3+} ions contributing to the spin-state transition than in $LaCoO_3$. Which Co^{3+} sites undergo the spin-state transition is addressed by the high-temperature structural study shown in the next section.

Because the spin-state transition of Co ions is always accompanied by a bond length change,[27,28] a high-temperature structural study is critical to clarify this uncertainty. Moreover, the structural study helps us to check the possibility of charge-order melting within the CdI_2-type layer. We therefore carried out high-temperature SXRD on $Ba_2Co_9O_{14}$ from 298 to 872 K over a broad range of the D space. Figure 7 displays the SXRD patterns in the range $5^\circ < 2\theta < 15^\circ$. As can be seen, no symmetry change can be discerned on crossing T_t. The detailed structural evolution as a function of temperature has been extracted by using Rietveld refinements on these SXRD patterns with a structural model[11] defined in the space group R-3m (No. 166), with the Ba atom at 6c (1/3, 2/3, z); five Co atoms at 6c (0, 0, z), 3b (0, 0, 1/2), 6c (2/3, 1/3, z), 9e (5/6, 1/6, 2/3), and 3a (1/3, 2/3, 2/3) sites; and three oxygen atoms located at 18h (x, y, z) and 6c (0, 0, z) positions. All refinements converged fairly well with

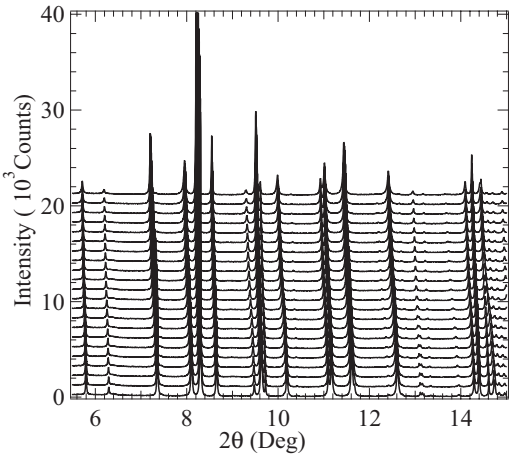

FIG. 7. High-resolution SXRD patterns of $Ba_2Co_9O_{14}$ in the 2θ range 5°–15° from 298 to 872 K.

TABLE I. Comparison of the unit-cell parameters, average ⟨Co-O⟩ bond lengths, and the BVS of Co ions at 298 K obtained in the present and the previous studies. The BVS model provides a phenomenological relationship between the formal valence of a bond and the corresponding bond lengths (Refs. 29 and 30). The valence S is the sum of the individual bond valences s_i for the Co-O bonds: $\mathrm{BVS} = \sum_i s_i = \sum_i \exp(r_0 - r_1)/B_0$, where $B_0 = 0.37$, $r_0 = 1.692$ for the Co^{2+}-O pair, and $r_0 = 1.637$ for the Co^{3+}-O pair.

$T = 298$ K		This work (SXRD)	Ref. 13 (SCD)	Ref. 14 (NPD)
a (Å)		5.69464(3)	5.6958(4)	5.6963(8)
c (Å)		28.9017(2)	28.909(4)	28.924(6)
Co1	⟨Co-O⟩	1.944(2)	1.937	1.935
Oct. (LS Co^{3+})	BVS	2.62(2)	3.00	3.18
Co2	⟨Co-O⟩	1.962(3)	1.954	1.945
Oct. (LS Co^{3+})	BVS	2.49(2)	2.86	3.09
Co3	⟨Co-O⟩	1.913(4)	1.922	1.931
Tet. (Co^{2+})	BVS	2.20(2)	2.15	2.10
Co4	⟨Co-O⟩	1.933(1)	1.919	1.915
Oct. (LS Co^{3+})	BVS	2.73(1)	3.15	3.36
Co5	⟨Co-O⟩	2.082(1)	2.076	2.082
Oct. (HS Co^{2+})	BVS	2.089(6)	2.12	2.09

typical reliability factors: $R_p \approx 10\%$, $R_{wp} \approx 12\%$, and $\chi^2 \approx 5.0\%$; the results are generally consistent with those obtained with both single-crystal diffraction (SCD)[13] and NPD.[14] The structural parameters at 298 K are listed in Table I, including the unit-cell parameters, average ⟨Co-O⟩ bond lengths, and calculated bond valence sum (BVS) for Co ions; the formula of the BVS is given in the footnote of Table I. The corresponding data from SCD[13] and NPD[14] are included in Table I for comparison. SXRD gives rise to high precision of the D space and therefore results in one more decimal in the lattice parameters in comparison with those obtained from SCD and NPD. However, diffractions with a wavelength $\lambda = 0.41219$ Å carry less information about the oxygen positions, especially the oxygen around Co^{3+}, than those in SCD and NPD, because the scattering to x-ray is sensitive to the total number of electrons. The less accurate Co-O bond lengths from SXRD lead to a relatively small BVS in Table I.

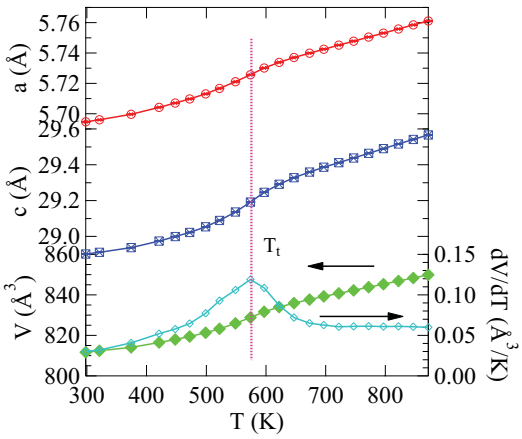

FIG. 8. (Color online) Temperature dependences of the unit-cell parameters a, c, V, and the temperature derivative dV/dT.

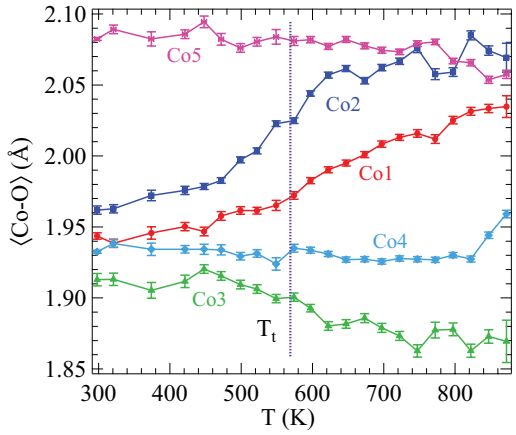

FIG. 9. (Color online) Temperature dependences of the average ⟨Co-O⟩ bond lengths for Co ions on different sites in $Ba_2Co_9O_{14}$.

Temperature dependences of the unit-cell parameters and the average ⟨Co-O⟩ bond lengths (d_{Co-O}) for all Co sites are shown in Figs. 8 and 9, respectively. Several important structural features can be clearly observed in the vicinity of T_t, which is marked by dotted lines: (1) an inflection point at T_t can be seen in all curves of a, c, and V vs T; (2) the bond lengths of d_{Co4-O} and d_{Co5-O} show no change or a slight decrease; and (3) d_{Co1-O} and d_{Co2-O} in the octahedral trimer expand dramatically in the vicinity of $T_t = 570$ K. The temperature dependence of the average d_{Co-O} for Co1 and Co2 from 300 to 800 K is not only out of the possible range of the thermal expansion in a typical perovskite oxide[25] but also significantly higher than the bond length change caused by the thermally driven LS to higher-spin transition in $LaCoO_3$[24] in which the transition remains incomplete for temperatures up to 1000 K.

The nearly temperature-independent d_{Co4-O} indicates that the trivalent Co4 ion does not contribute to the spin-state transition. On the other hand, the dramatic change of d_{Co1-O} and d_{Co2-O} on crossing T_t confirmed that the trivalent Co1 and Co2 ions within the octahedral trimer are responsible for the spin-state transition. The expansion of the Co_3O_{12} octahedral trimer due to the thermally driven spin-state transition also compresses the Co3-O tetrahedra that are connected via the corner-shared O1 to Co_3O_{12} trimer, leading to a concomitant shrinkage of the average d_{Co3-O} distance. The possibility of charge-order melting at T_t within the CdI_2-type layers can be readily excluded because the Co4 and Co5 ions can be well-distinguished by the large difference between their d_{Co-O} values in Fig. 9. However, the last few points of d_{Co4-O} at $T > 830$ K increase sharply, which may signal that the charge-ordering state within the CdI_2 layers of $Ba_2Co_9O_{14}$ is close to collapse at this temperature.

IV. CONCLUSION

The cobaltite $Ba_2Co_9O_{14}$ undergoes an insulator–insulator transition spreading over a broad range of temperatures around $T_t = 570$ K. The paramagnetic susceptibility deviates from a C-W law as T_t is approached from low temperatures. The thermoelectric power S indicates that $Ba_2Co_9O_{14}$ is a p-type polaronic conductor at $T < T_t$; an abrupt drop of S as temperature increases on crossing T_t indicates release of more

mobile charge carriers. There are five Co sites occupied by Co^{2+} and Co^{3+} in the crystal structure of $Ba_2Co_9O_{14}$. The Co-$L_{2,3}$ XAS spectrum reveals that the Co^{3+} ions have the LS state below 300 K. By using bulk-sensitive FY O-K XAS spectra, we show that a spin-state transition from the LS to a higher-spin state on Co^{3+} occurs at T_t. Structural details obtained from Rietveld analysis of high-temperature SXRD data help us to identify the specific Co^{3+} sites at the Co1 and Co2 where the spin-state transition takes place. Moreover, we find that the overall bond length change at these Co sites on crossing the spin-state transition is larger than the averaged Co^{3+}-O bond length change associated with the LS to higher spin transition found in $LaCoO_3$. Because the thermally driven spin-state transition in $LaCoO_3$ is incomplete at $T < 1000$ K, the saturation value of 2.05 Å found for the averaged Co1-O and Co2-O bond length in $Ba_2Co_9O_{14}$ could be used as a reference for HS Co^{3+} at octahedral sites. Finally, results from this structural study rule out the possibility of a collapse at T_t of the charge-ordered state in the CdI_2 structural layer containing Co4 and Co5 sites.

ACKNOWLEDGMENTS

This work was supported by the US National Science Foundation (Grants No. DMR 0904282, No. DMR 1122603, and No. CBET 1048767) and the Robert A. Welch Foundation (Grant No. F-1066). Use of the Advanced Photon Source at Argonne National Laboratory was supported by the US Department of Energy, Office of Science, Office of Basic Energy Sciences, under Contract No. DE-AC02-06CH11357.

*jszhou@mail.utexas.edu
†zhiwei.Hu@cpfs.mpg.de

[1] I. Terasaki, Y. Sasago, and K. Uchinokura, Phys. Rev. B **56**, R12685 (1997).
[2] K. Takada, H. Sakurai, E. Takayama-Muromachi, F. Izumi, R. A. Dilanian, and T. Sasaki, Nature (London) **422**, 53 (2003).
[3] A. C. Masset, C. Michel, A. Maignan, M. Hervieu, O. Toulemonde, F. Studer, B. Raveau, and J. Hejtmanek, Phys. Rev. B **62**, 166 (2000).
[4] D. Pelloquin, A. Maignan, S. Hebert, C. Martin, M. Hervieu, C. Michel, L. B. Wang, and B. Raveau, Chem. Mater. **14**, 3100 (2002).
[5] S. Sugano, Y. Tanabe, and H. Kaminura, *Multiplets of Transition-Metal Ions in Crystals* (Academic, New York, 1970).
[6] J. B. Goodenough, in *Progress in Solid State Chemistry*, edited by H. Reiss (Pergamon, Oxford, UK, 1971), Vol. 5.
[7] W. Koshibae, K. Tsutsui, and S. Maekawa, Phys. Rev. B **62**, 6869 (2000).
[8] A. Maignan, V. Caignaert, B. Raveau, D. Khomskii, and G. Sawatzky, Phys. Rev. Lett. **93**, 026401 (2004).
[9] Y. Diaz-Fernandez, L. Malavasi, and M. C. Mozzati, Phys. Rev. B **78**, 144405 (2008).
[10] C. Martin, A. Maignan, D. Pelloquin, N. Nguyen, and B. Raveau, Appl. Phys. Lett. **71**, 1421 (1997).
[11] L. Malavasi, Y. Diaz-Fernandez, M. C. Mozzati, and C. Ritter, Solid State Comm. **148**, 87 (2008).
[12] C. F. Chang, Z. Hu, H. Wu, T. Burnus, N. Hollmann, M. Benomar, T. Lorenz, A. Tanaka, H.-J. Lin, H. H. Hsieh, C. T. Chen, and L. H. Tjeng, Phys. Rev. Lett. **102**, 116401 (2009).
[13] J. Sun, M. Yang, G. Li, T. Yang, F. Liao, Y. Wang, M. Xiong, and J. Lin, Inorg. Chem. **45**, 9151 (2006).
[14] G. Ehora, S. Daviero-Minaud, M. Colmont, G. André, and O. Mentré, Chem. Mater. **19**, 2180 (2007).
[15] J.-Q. Yan, J.-S. Zhou, and J. B. Goodenough, Phys. Rev. B **69**, 134409 (2004).
[16] T. Takami, S. Saiki, J.-G. Cheng, and J. B. Goodenough, J. Phys. Soc. Jpn. **79**, 114713 (2010).
[17] J. Wang, B. H. Toby, P. L. Lee, L. Ribaud, S. Antao, C. Kurtz, M. Ramanathan, R. B. von Dreele, and M. A. Beno, Rev. Sci. Instrum. **79**, 085105 (2008).
[18] J. Rodriguez-Carvajal, Phys. B **192**, 55 (1993).
[19] J. Kanamori, Prog. Theor. Phys. **17**, 177 (1957).
[20] T. Burnus, Z. Hu, H. H. Hsieh, V. L. J. Joly, P. A. Joy, M. W. Haverkort, H. Wu, A. Tanaka, H.-J. Lin, C. T. Chen, and L. H. Tjeng, Phys. Rev. B **77**, 125124 (2008).
[21] Z. Hu, H. Wu, M. W. Haverkort, H. H. Hsieh, H.-J. Lin, T. Lorenz, J. Baier, A. Reichl, I. Bonn, C. Felser, A. Tanaka, C. T. Chen, and L. H. Tjeng, Phys. Rev. Lett. **92**, 207402 (2004).
[22] M. W. Haverkort, Z. Hu, J. C. Cezar, T. Burnus, H. Hartmann, M. Reuther, C. Zobel, T. Lorenz, A. Tanaka, N. B. Brookes, H. H. Hsieh, H.-J. Lin, C. T. Chen, and L. H. Tjeng, Phys. Rev. Lett. **97**, 176405 (2006).
[23] T. Burnus, Z. Hu, M. W. Haverkort, J. C. Cezar, D. Flahaut, V. Hardy, A. Maignan, N. B. Brookes, A. Tanaka, H. H. Hsieh, H.-J. Lin, C. T. Chen, and L. H. Tjeng, Phys. Rev. B **74**, 245111 (2006).
[24] M. Abbate, S. M. Lala, L. A. Montoro, and J. M. Rosolen, Phys. Rev. B **70**, 235101 (2004).
[25] N. Hollmann, Z. Hu, M. Valldor, A. Maignan, A. Tanaka, H. H. Hsieh, H.-J. Lin, C. T. Chen, and L. H. Tjeng, Phys. Rev. B **80**, 085111 (2009).
[26] M. Abbate, J. C. Fuggle, A. Fujimori, L. H. Tjeng, C. T. Chen, R. Potze, G. A. Sawatzky, H. Eisaki, and S. Uchida, Phys. Rev. B **47**, 16124 (1993).
[27] P. G. Radaelli and S.-W. Cheong, Phys. Rev. B **66**, 094408 (2002).
[28] Y. Ren, J.-Q. Yan, J.-S. Zhou, J. B. Goodenough, J. D. Jorgensen, S. Short, H. Kim, T. Proffen, S. Chang, and R. J. McQueeney, Phys. Rev. B **84**, 214409 (2011).
[29] N. E. Brese and M. O'Keeffe, Acta Crystallogr. B **47**, 192 (1991).
[30] I. D. Brown, Z. Kristallogr. **199**, 255 (1992).